Nondestructive Testing and Evaluation,
Vol. 23, No. 2, June 2008, 109–120

Nondestructive testing of open microscopic cracks in plasma-sprayed-coatings using ultrasound excited vibrothermography

JEAN-MARC PIAU†*, ABDELHAKIM BENDADA†, XAVIER MALDAGUE† and JEAN-GABRIEL LEGOUX‡

†Computer Vision and Systems Laboratory, Laval University, Quebec City, Quebec, Canada, G1K 7P4
‡Research Officer, Surface Technologies, NRC Industrial Materials Institute (IMI), National Research Council of Canada (NRC), 75 de Mortagne Boulevard, Boucherville, Quebec, Canada, J4B 6Y4

(Received 6 June 2007; in final form 7 November 2007)

While other nondestructive testing methods hardly reveal microscopic open cracks, vibrothermography stimulated by ultrasound provides very promising results by converting mechanical waves into local heat by friction. This phenomenon enhances thermal gradients in temperature maps as compared to conventional techniques. To detect temperature gradients caused by hidden cracks, high thermal and spatial resolution infrared cameras are usually used. The aim of this work is to investigate the ability of the vibrothermography stimulated by ultrasound to detect such cracks and measure the gap between adjacent cracks. To do so, we investigated tungsten carbide coatings where cracks were artificially generated using a controlled bending test. Several samples were investigated during this study but only typical results from one sample are presented and discussed.

Keywords: Nondestructive evaluation; Ultrasound excited vibrothermography; Microscopic open cracks

1. Introduction

Recently, it has been shown that the high velocity oxy fuel (HVOF) spraying of tungsten carbide or cobalt coatings onto steel substrates seems to be a suitable alternative to the non-environmentally friendly chromium coating material. However one major issue with these plasma-sprayed-coatings is the possibility of the appearance of open microscopic cracks when they are submitted to excessive bending loads. For clarity reasons, it should be pointed out here that an open crack is a surface breaking crack. If the open cracks spread through the whole coating thickness, crack propagation to the coating–substrate interface might cause the coating to delaminate in between adjacent open cracks. The latter disbonding phenomenon is therefore strongly dependent on the distance between adjacent open cracks. Therefore, a nondestructive technique enabling the detection of cracks and the evolution of their density is critical to preserve the components integrity.

*Corresponding author. Email: jmpiau@gel.ulaval.ca

Nondestructive Testing and Evaluation
ISSN 1058-9759 print/ISSN 1477-2671 online © 2008 Taylor & Francis
http://www.tandf.co.uk/journals
DOI: 10.1080/10589750701775817

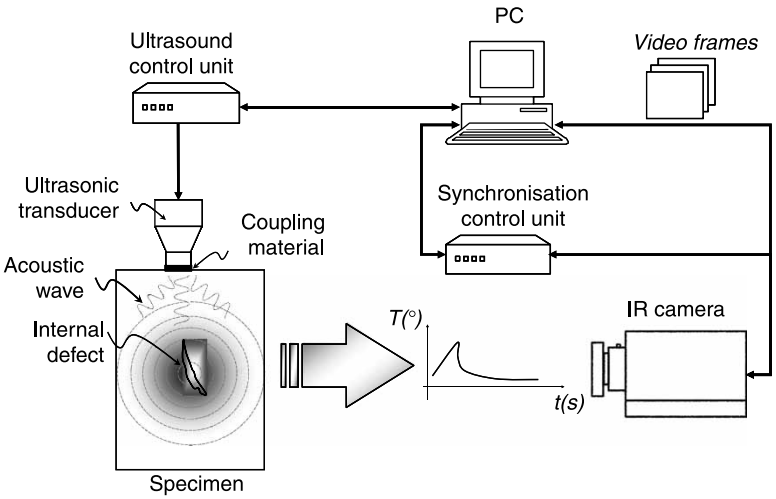

Figure 1. Ultrasound vibrothermography setup.

In this paper, we present an application to detect microscopic open cracks using an ultrasound vibrothermography (UVT) detection technique. UVT is also known as thermosonics, or ultrasound thermography, and relies on the conversion of mechanical elastic waves into heat. Ultrasonic waves travel freely through homogeneous materials, whereas inhomogeneities produce complex combinations of absorptions, scatterings, beam spreading and dispersions of the waves, whose principal manifestation will be in the form of a heat source. More physically, the main mechanisms involved are due to thermoelasticity, viscoelasticity and friction (Meyendorf *et al.* 2002). So, inhomogeneities are mainly considered as defects in a structure. They thus convert elastic waves into a heat source, yielding a precise heat localisation. Heat locally released propagates by conduction toward the surface where it can be mapped spatially and time wise with an infrared camera. Figure 1 presents the standard UVT setup used. Ultrasound frequency range allows the stress level to be reduced with sufficient detectable thermal energy as compared to the stress pattern analysis by thermal emission (SPATE) technique (Harwood and Cummings 1991). Ultrasounds are not audible to humans, however lower frequencies appear due to the non linear effect at the ultrasound injection point (Solodov 1998; Han *et al.* 2002). Microscopic open cracks, created by bending tests to accelerate the aging process, corrupt the coating integrity by forming discontinuities. These discontinuities can be described as a fracture of two edges starting from the surface; some might propagate down to the steel interface. At rest, when the bending load is removed, cracks tend to close up thus rubbing or clapping of fracture edges is likely to happen under ultrasonic stimulation.

2. Experimentation setup

The ultrasound source used for the experimentation is derived from an industrial plastic welder unit modified to generate elastic waves from 15 to 25 kHz. As shown in figure 2, an electrical signal generated from the controller feeds the piezo. A booster is screwed onto the piezo's end to concentrate the ultrasound wave to a surface of 30 mm in diameter. Home-made software has been developed to generate customised electrical waveforms.

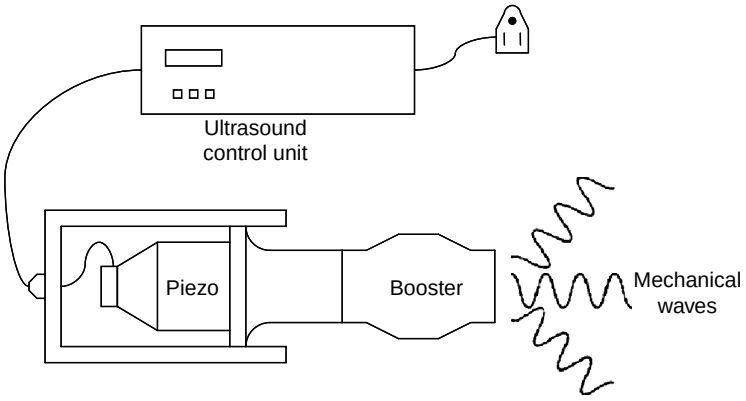

Figure 2. Ultrasound source.

The sample is pressed between the titanium ultrasound booster and a hard insulation post made of aluminum ended by a Teflon® tip. The holding pressure has a strong influence on the thermal response (Perez and Davis 2003). In this experiment, the pressure was set to 50 PSI, just strong enough to hold the sample and avoiding any displacement of the sample during the ultrasound stimulation. The pressure applied by the pneumatic pistons is digitally monitored for experimental reproducibility. Sample dimensions and weight allow having a single insulation contact at one end while leaving the other end in free motion. A cork slice was inserted between the insulation post and the sample. The size of the cork slice in contact with the sample was thoroughly determined by empirical trials until optimum defect detectability was achieved. A coupling material can be inserted between the titanium booster and the sample to improve ultrasound transfer into the sample, the impedance matching is described in detail by Zweschepe*r et al.* (2003). A wet tissue was used; this soft material also compensates for surface misalignment and protects the sample surface from fretting. Ultrasounds are injected on the back side of the sample and the infrared camera is facing the tungsten carbide coating. If only one side is accessible, ultrasound injection on the coating side is also possible. The latter configuration gives the same results but the setup is more complex. This additional complexity is caused by the issue of physically arranging the camera to point directly toward the area of interest of the sample. The large sizes of the booster and the piezo, and the small size of the sample are the reasons of this additional complexity. To overcome the latter issue, we installed an infrared mirror in order to reflect out the infrared images of the coating toward the camera. It should be mentioned here that in real-life the parts to inspect are much larger than the academic samples described during the current study. Indeed, for such parts ultrasounds can be injected farther away from the inspected area since the parts material is a good ultrasound propagating medium. The experimental arrangement used in our experiments is schematically represented in figure 3; in order to allow all the components to be clearly seen, it is represented when the pressure is not applied. The infrared camera is an InSb Phoenix® Indigo, 14 bits, operating in the 3–5 μm wavelength range, with a spatial resolution of 512 × 640 pixels, and a temperature resolution of 20 mK. During our experiments, the integration time was set to 0.8 ms. The 1 × macro-lens attached to the camera allows the visualisation of a maximum area of 16 × 12.8 mm (pixel size of 25 μm). Tests have also been done with a wide angle lens that has a focal point of a few centimeters, the whole sample was visualised but the poor

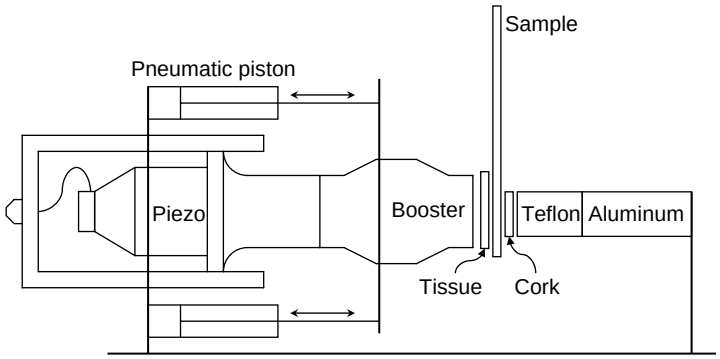

Figure 3. Experimentation approach.

resolution did not reveal the open cracks. However, it was useful to see the undesired heat around the ultrasound injection point.

By changing the coupling configuration from one experiment to another, we noticed that crack detectability decreased drastically, i.e. worse contrasts, when the undesired heat produced by the exciter tip was high (typically a 2–3°C temperature rise was monitored with a thermocouple). An explanation for such a phenomenon could be that when the coupling is bad, ultrasound energy is not well transferred into the bulk of the sample, i.e. toward the cracks, but rather dissipated into heat in the vicinity of the injection point.

After preliminary tests, the best detectability was observed with the ultrasound frequency source set to 20 kHz. No frequency modulation stimulation was necessary since the sample did not suffer from standing wave patterns. Standing waves are generally undesired because they might hide flaws with their regular patterns, but if flaws are geometrically important, the regularity of the standing wave patterns are disturbed which can lead to a kind of detection.

3. Sample description

HVOF is a supersonic process spraying molten droplets of coating material at extremely high velocities. The coating is formed by a mixture of Tungsten–Carbide and Cobalt powder accelerated and heated into a plasma jet and sprayed onto a 1-mm-thick steel substrate. Fuel and oxygen are fed into a chamber; combustion produces a hot high pressure circular flame which is forced down a nozzle increasing its velocity (typically 600–700 m/s). Popular fuel gases include Hydrogen, Propylene, Acetylene, and Kerosene. The resulting coating is very dense, very well bonded, and free of the oxides and tensile stresses typically found in coatings provided by other thermal spray processes. HVOF wear resistant surfaces typically provide more than four times the wear resistance of chrome plating, through hardening and other hard facing techniques. Their use is increasing worldwide for environmental reasons and due to their superiority over chromium coating. The thickness of the coating layer is typically ranging from 100 to 200 μm. Thermally sprayed coatings are formed by stacking of individual lamellae whose interfacial thermal contact is limited by the presence of pores or secondary phases (Moreau *et al.* 1993).

Six Almen strips were supplied by the National Research Council of Canada, but only results from one sample are presented hereafter. Figure 4 shows the latter sample whose dimensions are 76.2 mm × 19.2 mm. The sample was maintained by four holding clips

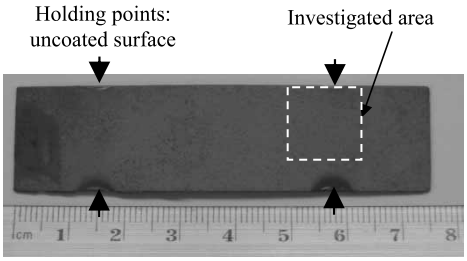

Figure 4. Tungsten carbide Almen strip.

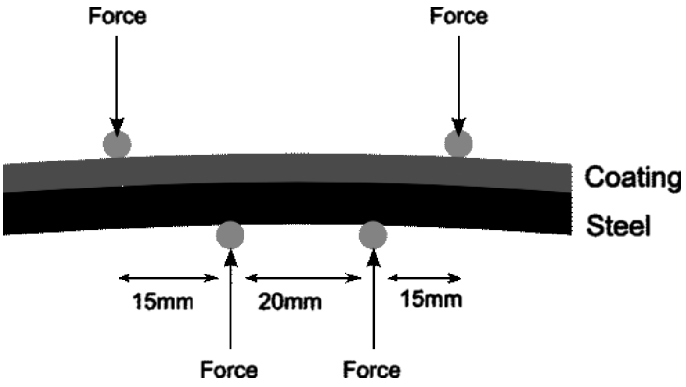

Figure 5. Four-point-bending specification.

during the HVOF process. This left four semi-circular uncoated areas at the edges; they are identified with black arrows in figure 4. Coating resistance testing is carried out by applying a mechanical load according to a four-point-bending-test as described in figure 5 until the formation of cracks begins. The presence of cracks is monitored during the bending by acoustic emission with a microphone in contact with the sample. These cracks can propagate down to the substrate and might cause delamination if the spacing between cracks is too small. Samples are not likely to be identical; each sample has a different crack pattern (size, depth and spacing). The samples have been tested without any conditioning, i.e. no high emissivity painting was applied, since the tungsten carbide coating has an emissivity around 0.96 in the spectral sensitivity range of the infrared camera.

4. Experimentation

Two types of stimulations were experimented to reveal the thermal signature of the open cracks. First, the pulse method which consists in delivering ultrasound during a short time, generally between 25 and 500 ms at constant amplitude. Cracks are visible directly from the raw thermograms. With fast recording frequency acquisition at 93 Hz full resolution (640×512), it is possible to record the temperature increase with a good time resolution. The longer the excitation, the higher the gradient and thus the longer the cooling down. A set of plots is presented in figure 6.

The second excitation method consists of modulating the ultrasound power amplitude and synchronising the acquisition with the stimulation like the lock-in method (Rantala *et al.* 1996). Long acquisition time and amplitude modulation frequency selections are the main

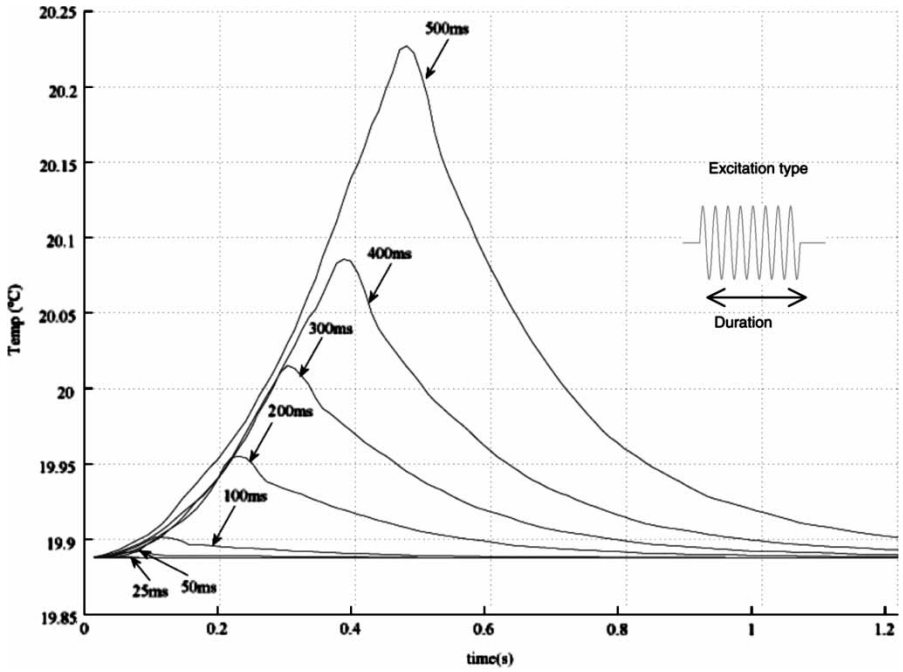

Figure 6. Gradient profile (Temperature versus time). Pulse duration: 25, 50, 100, 200, 300, 400, and 500 ms.

drawbacks. The experiments performed differ from the conventional lock-in, the acquisition is done during the transient regime and the stimulation only lasts three periods. The amplitude modulation frequency was set to 2 Hz. Figure 7 presents two typical crack surface gradient profiles (a,b) and the bottom curve (c) is a sound region gradient profile taken between cracks. One can see the transient regime with the three pseudo sinusoidal periods ramping up followed by the cooling down which has not been recorded entirely.

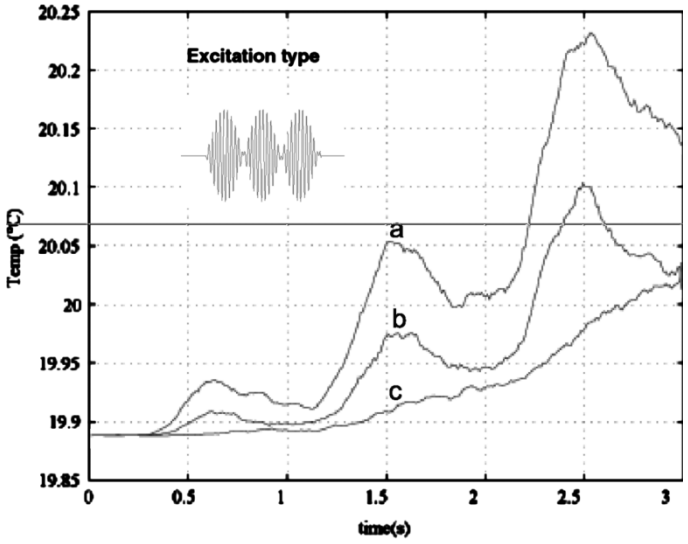

Figure 7. Temperature versus time transients (modulation at 2 Hz). (a,b) Temperature versus time transients on two different cracks. (c) Temperature versus time transient in between two cracks.

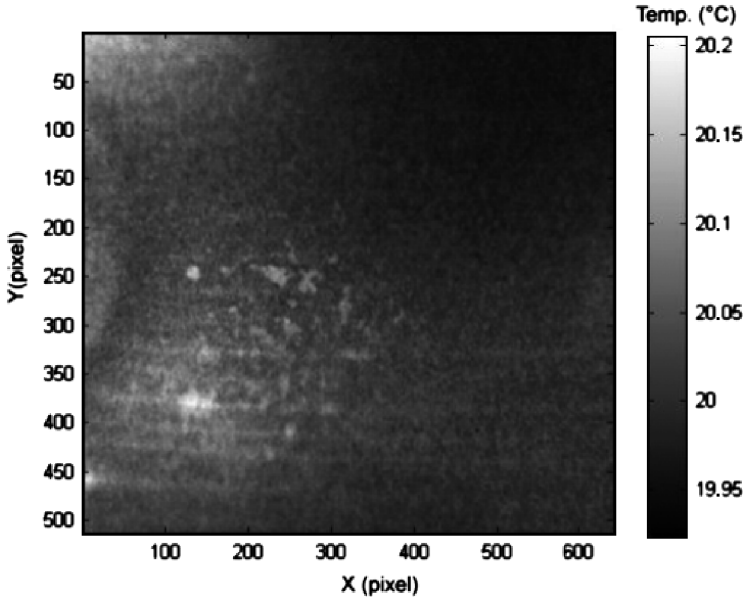

Figure 8. Raw temperature image. Pulse stimulation: pulse duration of 500 ms.

Image processing can be used to improve data interpretation; magnitude and phase thermograms obtained by Fast Fourier Transform (FFT; Maldague and Marinetti 1996) gave better contrasts. Acquisition performed with amplitude modulation stimulation required the FFT phase image processing; however raw images obtained with pulse stimulation gave relatively decent pictures for a quick evaluation (figure 8). The recorded sequence was processed by first subtracting a cold image, i.e. an image obtained a few frames before the stimulation, and then phasegrams were generated by IR-View (Klein 1999). IR-View is a tool designed specifically to analyze infrared nondestructive testing images. Truncation of the infrared sequence might sometimes be necessary to keep only the heating up regime; no signal de-noising filters were applied. Figure 9 is an example of a phase thermogram also called phasegram; one can see clearly the horizontal black strips which locate the open cracks. The area investigated is shown in figure 4. The bright semi-circle on the left-hand-side is one of the holding points used during the coating process; as a consequence, this region is not coated. Edges of the specimen are likely to present high contrasts. Other material investigations proved that the edges of the inspected specimen should be considered with caution before drawing any conclusions with respect to defects on edges.

5. Vibration into the specimen

The use of a laser vibrometer indicates that the specimen is vibrating not only at the selected ultrasound frequency (20 kHz). A rather complex frequency spectrum is obtained by conducting a FFT signal analysis on the vibration signal recorded during the stimulation. Harmonics and sub-harmonics appear with different amplitudes spreading from a few Hertz up to 100 kHz. Clamping the specimen or not to maintain it in position changes the frequency spectrum response. Certain frequencies appear stronger when the sample is clamped and some others vanish. Figure 10(A) shows the frequency spectrum of the recorded vibration;

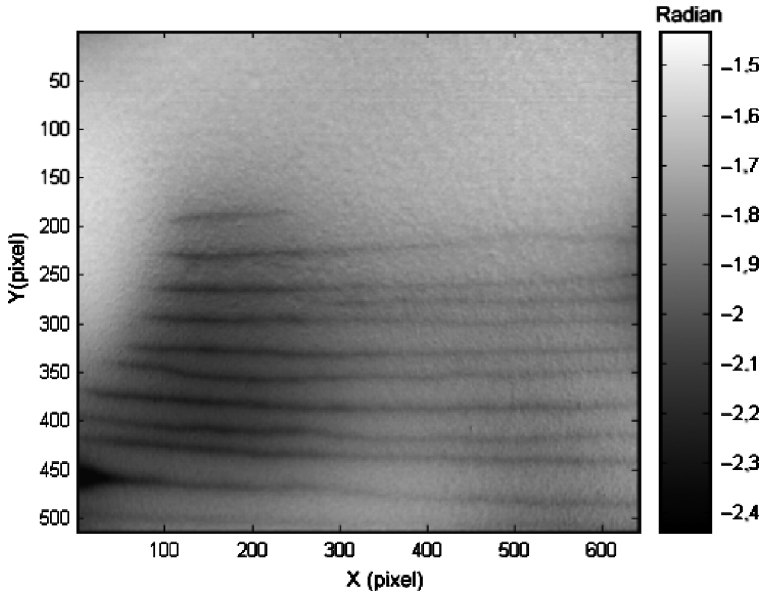

Figure 9. Phasegram image. Modulated stimulation: amplitude modulated at 2 Hz.

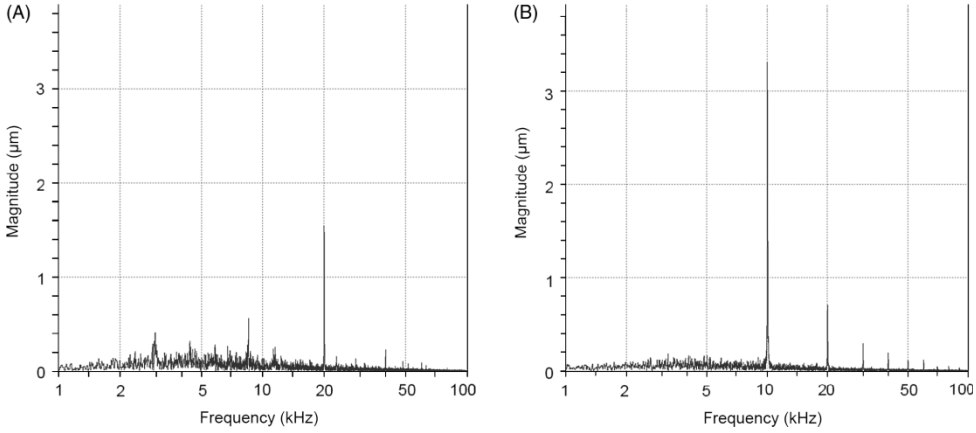

Figure 10. (A) Frequency spectrum with sample not clamped. (B) Frequency spectrum with the sample clamped at the top.

the ultrasound stimulation was a 100 ms pulse. The laser was pointed in the same region investigated by thermography. When the sample is mechanically clamped at its top end, one can notice on the frequency spectrum in figure 10(B) that the energy is distributed differently, and a strong peak appears at 10 kHz. Frequency spectrum analysis is beyond the scope of this article; for more detailed information we refer the reader to Han *et al.* 2002. Furthermore, it is worth noticing from figure 10 that frequencies under the human hearing limit are present. So for safety reasons, hearing protection is strongly recommended.

Cracks do not respond specially at the stimulation frequency and it is difficult to predict which vibration frequency is best suited for the conversion of acoustic energy into heat. When the frequency spectrum is spread over several frequencies, the chances of a good detection increase.

6. Results

The area investigated presents open cracks; they are all oriented in the same direction (figure 11). Cracks show different contrast levels. To perform the crack spacing measurements, two phase profiles (column A and column B) have been extracted (figure 12) from the phasegram image of figure 11. A peak detection procedure allows cracks to be accurately located on the *Y*-axis. Lines have been drawn passing through paired peaks to show the direction of the cracks. Finally, circles and crosses in figure 11 have been displayed according to the *Y* coordinate found by the peak detection; this verifies, visually, the exactitude of the detection. With the lens specification and camera pixel size, crack spacings have been accurately converted into millimeters. In order to validate the location and type of cracks, a sample was irreversibly cut to perform electronic microscope photography depth wise. The investigated cracks have been numbered from 1 to 10 as shown in figure 11. Figures 13 and 14 report the error difference distance between neighboring

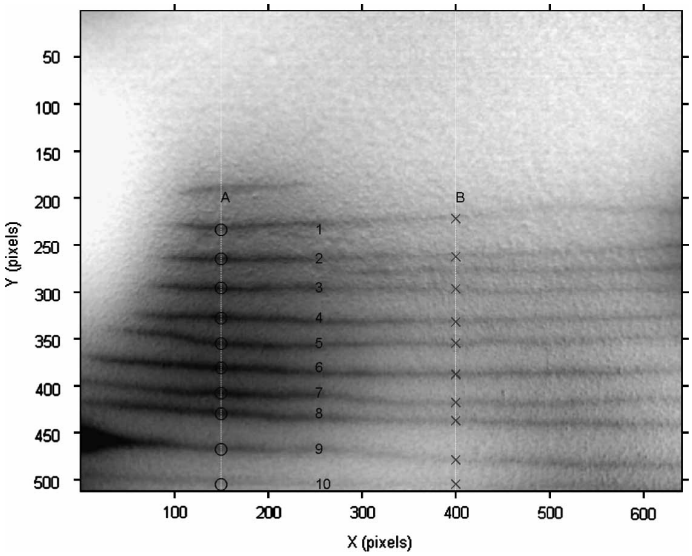

Figure 11. FFT, Phasegram, 2 Hz. (A) Column 150. (B) Column 400.

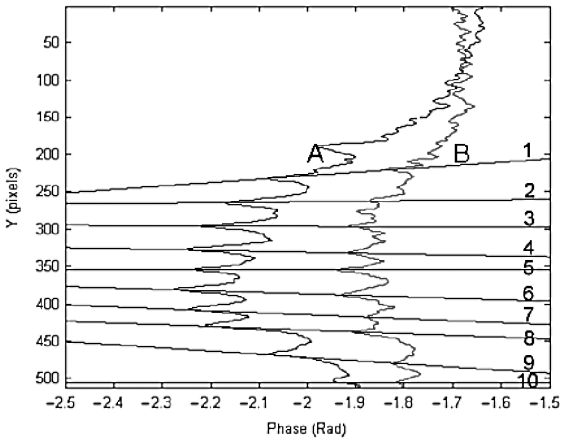

Figure 12. Phase profiles (Columns A and B). (A) Column 150 (B) Column 400.

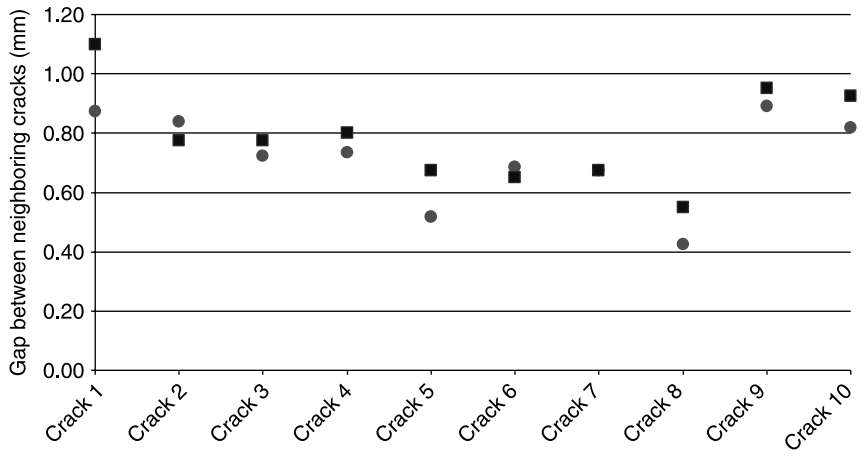

Figure 13. Crack spacing comparison of column A. ● Thermography ■ Microscope.

cracks observed by both techniques. One of the investigated cracks with microscopic photography is shown in figure 15. The gap between the crack edges is in the nanometer order. This electronic microscope image covers the region from the surface down to the steel interface (approximately 200-μm-height, 125-μm-width). The crack might not look straight from the top to the bottom but considering the scale it does not matter much for the measurement purposes and the surface heat is taken at its peaks for each crack. Smaller cracks, a few tenths of a micrometer deep from the surface, were observed between deep cracks with electronic microscope inspection. Those smaller cracks were however not detected with ultrasound excited thermography. But it should be mentioned here that the latter cracks do not affect the coating wear resistance that much since the risk of coating delamination is not that big compared to deep cracks reaching the substrate.

Calibration of the infrared acquisition system with a black body and determination of the tungsten carbide emissivity allows the surface temperature to be calculated. A temperature difference of 200 mK between adjacent cracks was measured. For this particular investigated area, the electronic microscopic imaging inspection has revealed that cracks close to the edge (left-hand-side in figure 11, vicinity of Column A) present more ramified patterns.

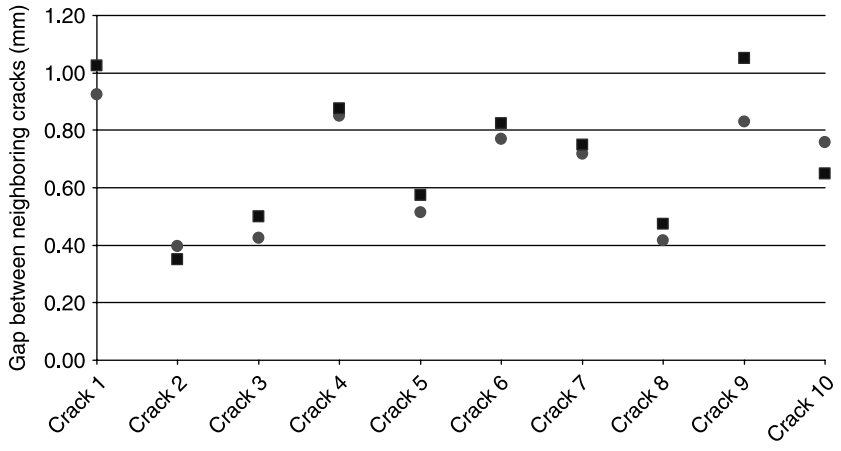

Figure 14. Crack spacing comparison of column B. ● Thermography ■ Microscope.

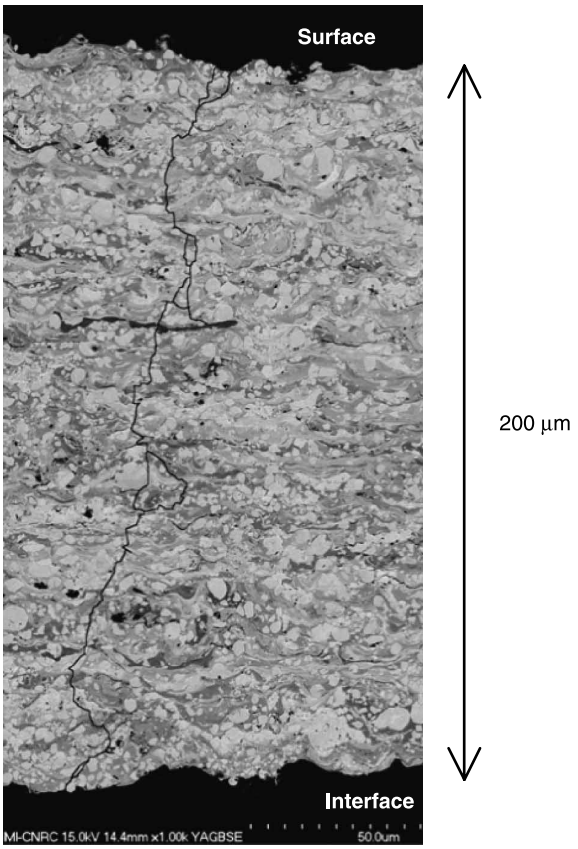

Figure 15. Microscopic image of a crack.

Furthermore, the coating thickness is 20 μm lower than the thickness in the middle of the specimen (i.e. in the vicinity of Column B). The latter two observations could explain the contrast difference along the length of the same crack.

7. Conclusion

UVT is an excellent, fast, repeatable and reliable technique to detect open microscopic cracks in plasma-sprayed-coatings. As far as we know, no other nondestructive technique seems to reveal such nanometer wide cracks. For instance, optically excited lock-in and pulsed thermography inspection experiments carried out in our laboratory on the same samples failed to reveal any crack. With ultrasound excited thermography, cracks spreading all the way through the coating were successfully detected but shallow cracks were not. The latter cracks do not reach the coating–substrate interface and therefore would not cause any disbonding damage of the coating. It should be mentioned here that the depth detection limit could not have been established with the specimens at hand since all shallow cracks were located at almost the same depth from the surface, i.e. at 20 μm, as observed with electronic imaging inspection. Due to the size of the cracks, the use of a macro-lens is required, thereby dramatically reducing the inspected area, however stitching image techniques allow a wider area to be covered after several acquisitions.

The repeatability of crack detection is highly guaranteed if the coupling, holding pressure and insulation surface are meticulously adjusted. Modulated amplitude ultrasound excitation gave better images than pulse amplitude ultrasound excitation. Raw images are often sufficient to locate most of the cracks but detection is highly improved by image processing methods such as FFT. No crack growth has been monitored even with intensive testing. In the future, we intend to develop inverse algorithms based on heat transfer models and infrared imaging to estimate crack propagation within the coating. We also plan to develop a new four-point-bending-test setup which allows real-time-vision of crack propagation during the test itself.

Acknowledgements

We gratefully acknowledge Dr Jean-Gabriel Legoux and the Surface Technology Group from the National Research Council of Canada, who provided us with the Tungsten–Carbide and Cobalt coated Almen samples and precious help with the microscopic images.

References

Han, X., Li, W., Zeng, Z., Favro, L.D. and Thomas, R.L., Acoustic chaos and sonic infrared imaging. *Appl. Phys. Lett.*, October 2002, **81**(17), 3188–3190.

Harwood, N. and Cummings, W.M., *Thermoelastic Stress Analysis*, 1991 (Adam Hilger: Bristol, Philadelphia, and New York).

Klein, M., 1999, http://irview.m-klein.com, Laboratoire de vision et systèmes numériques, Dép. de génie électrique, Université Laval, Québec City, Québec, Canada, G1K 7P4, Last Update: 03-2007.

Maldague, X.P. and Marinetti, S., Pulse phase infrared thermography. *J. Appl. Phys.*, 1996, **79**(5), 2694–2698.

Meyendorf, N.G.H., Rosner, H., Kramb, V. and Sathish, S., Thermo-acoustic fatigue characterization. *Ultrasonics*, May 2002, **40**(1–8), 427.

Moreau, C., Fargier-Richard, P., Saint-Jacques, R.G. and Cielo, P., Thermal diffusivity of plasma-sprayed tungsten coatings, International conference on metallurgical coatings and thin films, No. 20, April 1993, San Diego CA, USA, **61**(1–3), 67–71.

Perez, I. and Davis, W.R., Optimizing the thermosonics signal. *Proceedings of the AIP Conference*, Cambridge, MA, USA, November 2003, **657**, 505–512.

Rantala, J., Wul, D. and Busse, G., Amplitude-modulated lock-in vibrothermography for NDE of polymers and composites. *Res. Nondestruct. Eval.*, December 1996, **7**(4), 215–228.

Solodov, I.Y., Ultrasonics of non-linear contacts: propagation, reflection and NDE-applications. *Ultrasonics*, February 1998, **6**(1–5), 383–390.

Zwescheper, T., Dilenz, A., Riegert, G., Sherling, D. and Busse, G., Ultrasound excited thermography using frequency modulated elastic waves. *Insight*, March 2003, **45**(3), 178–182.